Picosecond polarized fluorescence studies of anisotropic fluid media. II. Experimental studies of molecular order and motion in jet aligned rhodamine 6G and resorufin solutions

A. J. Bain, P. Chandna, G. Butcher, and J. Bryant

Articles you may be interested in

Two-photon-excited fluorescence resonance energy transfer in an aqueous system of CdTe quantum dots and Rhodamine B
J. Appl. Phys. **116**, 233106 (2014); 10.1063/1.4904356

Fluorescence quenching of rhodamine-6G in Au nanocomposite polymers
J. Appl. Phys. **108**, 084311 (2010); 10.1063/1.3496668

Experimental study of foam jets
Phys. Fluids **22**, 033302 (2010); 10.1063/1.3335816

Identifiability analysis of models for reversible intermolecular two-state excited-state processes coupled with species-dependent rotational diffusion monitored by time-resolved fluorescence depolarization
J. Chem. Phys. **121**, 7829 (2004); 10.1063/1.1798972

Picosecond polarized fluorescence studies of anisotropic fluid media. I. Theory
J. Chem. Phys. **112**, 10418 (2000); 10.1063/1.481678

Picosecond polarized fluorescence studies of anisotropic fluid media. II. Experimental studies of molecular order and motion in jet aligned rhodamine 6G and resorufin solutions

A. J. Bain,[a),b)] P. Chandna, G. Butcher,[c)] and J. Bryant[b)]

Department of Physics, University of Essex, Wivenhoe Park, Colchester, C04 3SQ, United Kingdom

New polarized time resolved fluorescence techniques are implemented to determine the full angular motion of a probe molecule in an anisotropic environment. Studies of rhodamine 6G and resorufin molecules aligned in a free ethylene glycol jet show that the presence of net molecular order is accompanied by a distinct anisotropy in alignment relaxation following photoselection. Diffusion coefficients for ϕ and θ motion ($D_\parallel$ and $D_\perp$) in a jet fixed axis system are determined from the cylindrically symmetric and asymmetric alignment relaxation rates for the isotropic and anisotropic regions of the jet. The presence of net negative molecular alignment as the free jet is formed is seen to correspond to restricted ϕ motion ($D_\parallel < D_\perp$), with a net positive steady state alignment the anisotropy in the diffusion dynamics is reversed. The differences in $D_\parallel$ and $D_\perp$ are attributed to anisotropy in the solvent viscosity as a consequence of flow. The combination of linear and circular polarization techniques is seen to provide useful information on cylindrical asymmetry and relaxation dynamics hitherto unobserved by conventional fluorescence polarization techniques. © *2000 American Institute of Physics.* [S0021-9606(00)00217-8]

I. INTRODUCTION

In the first paper of this series (Paper I) we developed a formalism for treating the interaction of polarized laser pulses with an anisotropic molecular array allowing, for an array of given asymmetry, a full characterization of the initial excited state orientational distribution function. The subsequent evolution of the excited state in the anisotropic environment was considered in terms of a perturbation solution to the anisotropic diffusion equation and the form of the alignment decays which comprise the experimentally measured single photon fluorescence anisotropy can be predicted. It was further shown that for a system with axial symmetry a number of specific excitation polarization conditions could be employed which individually highlight the symmetric and asymmetric alignment dynamics. In this second paper we employ these techniques to investigate the steady state order and anisotropic orientational motion of rhodamine 6G and resorufin molecules in a free ethylene glycol jet. Preliminary jet experiments had revealed the presence of substantial molecular order to be accompanied by a distinct anisotropy in θ and ϕ diffusion dynamics indicating a breakdown in the ''selection rules'' for isotropic orientational relaxation.[1,2] In this work we are able to quantify these observations and to determine the functional form of the orientational correlation functions for the cylindrically symmetric and asymmetric degrees of the photoselected molecular alignment and to measure their characteristic relaxation rates.

These measurements are performed in different regions of the jet (corresponding to varying degrees of steady state molecular alignment) allowing an investigation into the nature of the θ and ϕ diffusional anisotropy with steady state order.

II. MOLECULAR ALIGNMENT AND MOTION IN FLUID MEDIA

The imposition of molecular order in an otherwise isotropic fluid medium requires the imposition of external forces to counteract the randomizing effects of Brownian motion. Traditionally this has been achieved in two distinct ways, first, by the imposition of shear forces arising from confined fluid flow[3–7] and second by the use of an applied dc electric field on a polar or anisotropically polarizable molecular system.[8–10] The result of these approaches is to create an energy difference between differing molecular orientations (θ,ϕ) defined relative to a laboratory axis system, which for a system in thermal equilibrium with its surroundings gives rise to the well known expression for the orientational distribution function,

$$P(\theta,\phi) = \frac{1}{Z}\exp\left(-\frac{E(\theta,\phi)}{kT}\right), \tag{2.1}$$

where Z is the orientational partition function for the system.[11] Following Paper I, $P(\theta,\phi)$ can be expressed as a multipolar expansion whose moments are given by

$$\langle C_{KQ}\rangle = \frac{1}{Z}\int_0^{2\pi}\int_0^{\pi} Y_{KQ}^*(\theta,\phi)\exp\left(-\frac{E(\theta,\phi)}{kT}\right)\sin\theta\, d\theta\, d\phi. \tag{2.2}$$

In the case of Couette flow, the energy of orientation of the symmetry axis of an ellipsoidal molecule relative to the flow direction z leads to an orientational distribution function according to[5,6]

$$P(\theta,\phi)=\frac{1}{4\pi}\left(1+\frac{\lambda A}{4D}\cos 2\theta \sin 2\phi\right). \quad (2.3)$$

Here λ is the applied shear, D is the isotropic rotational diffusion coefficient of the major axis, and A is an asymmetry parameter defined in terms of the major and minor semi-axes of the molecular ellipsoid of inertia a and b according to $A=(a^2-b^2)/(a^2+b^2)$. For small to medium sized molecules D is several orders of magnitude greater than the value of λ obtainable in a traditional Couette apparatus[6] and as such the technique is almost wholly restricted to slowly diffusing macromolecular assemblies.[6] In the case of electric field or Kerr alignment a purely dipolar interaction between the molecular dipole moment $\boldsymbol{\mu}$ and the applied field $\mathbf{E}$ of the form $E(\theta,\phi)=-\mu E\cos\theta$ leads to a degree of steady state alignment given by

$$\langle\alpha_{20}\rangle=\frac{\langle C_{20}\rangle}{\langle C_{00}\rangle}=\sqrt{5}\left[1+\frac{3}{a^2}\left[1-a\frac{\cosh a}{\sinh a}\right]\right], \quad (2.4)$$

where $a=\mu E/kT$. Ionic species such as rhodamine 6G and resorufin have large permanent dipole moments ($\approx$10–20 D) in solution, taking 20 D as an upper bound to μ together with an upper limit to E of $\approx$30 kV cm^{-1} yields a maximum value for $\langle\alpha_{20}\rangle$ of 1.56×10^{-3}. Uncharged but highly polar molecules of a similar size to rhodamine 6G and resorufin have lower dipole moments by at least an order of magnitude and the degree of Kerr alignment attainable in these instances will be still smaller yielding $\langle\alpha_{20}\rangle$ values in the range of 10^{-4}–10^{-5}.[9,10] If this favorable degree of ordering were to be carried through to the excited state then the relaxed or steady state fluorescence anisotropy R_{ss} observed [see Paper I, Eq. (7.8)] should be in the range of $10^{-3}\%$–$10^{-4}\%$. Significant molecular alignment using dc electric fields has only been achieved in larger and more polarizable species such as macromolecules[11] and systems exhibiting collective responses such as liquid crystals.[12,13]

The observation of possible molecular alignment in a free fluid jet was first reported by McCaffery and co-workers[14,15] who observed a spatial variation in the continuous wave fluorescence anisotropy from rhodamine 6G molecules in an ethylene glycol jet produced from a precision sapphire nozzle. Our initial time resolved polarized fluorescence measurements on this system[1,2] have shown that irrespective of the initial photoselection, the steady state ordering of the emerging molecules (R_{ss}) corresponds to a marked perpendicular (negative) alignment to the flow direction. The degree of this alignment is between one to three orders of magnitude greater than that attainable for similar species under favorable Couette or Kerr alignment conditions (as above).

In this work a more detailed study of molecular motion and order in the jet is undertaken using the formalism developed in Paper I. Our investigations are extended to include, in addition to the oblate rotor rhodamine 6G, the faster diffusing symmetric prolate rotor resorufin. Both molecules
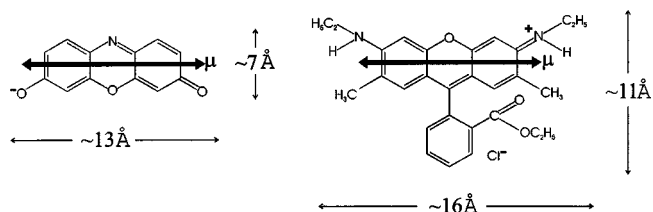

FIG. 1. The molecular structure and approximate dimensions of rhodamine 6G and resorufin. The direction of the (parallel) absorption and emission transition dipole moments μ are also indicated. In the case of rhodamine 6G, μ is orthogonal to the oblate symmetry axis (out of the plane of the paper), whereas for resorufin μ is collinear with the prolate symmetry axis.

have approximately parallel visible absorption and emission transition dipole moment directions (illustrated in Fig. 1), in the case of rhodamine 6G these are at 90° to the oblate symmetry axis and in principle the fluorescence anisotropy in isotropic media should show a biexponential decay according to[16,17]

$$R(t)=0.3\exp(-(4D_\parallel^M+2D_\perp^M)t)+0.1\exp(-6D_\perp^M t), \quad (2.5)$$

where $D_\parallel^M$ and $D_\perp^M$ are the (molecule fixed) coefficients for diffusion parallel and perpendicular to the molecular symmetry axis. Providing the difference between $D_\parallel^M$ and $D_\perp^M$ is not substantial, the anisotropy decay from an oblate rotor such as rhodamine 6G approximates well to a single exponential of the form,[18]

$$R(t)=0.4\exp(-3(D_\parallel^M+D_\perp^M)t). \quad (2.6)$$

In the case of resorufin, the transition dipole moment direction is directed along the prolate symmetry axis and a single exponential decay involving solely $D_\perp^M$ is observed,[16]

$$R(t)=0.4\exp(-6D_\perp^M t). \quad (2.7)$$

Both molecules are seen to exhibit single exponential fluorescence anisotropy decays in ethylene glycol (Fig. 2) where their orientational dynamics fall between the stick and slip limits of continuum hydrodynamics.[19] Their appropriate structural parameters and isotropic diffusion rates in ethylene glycol are given in Table I.
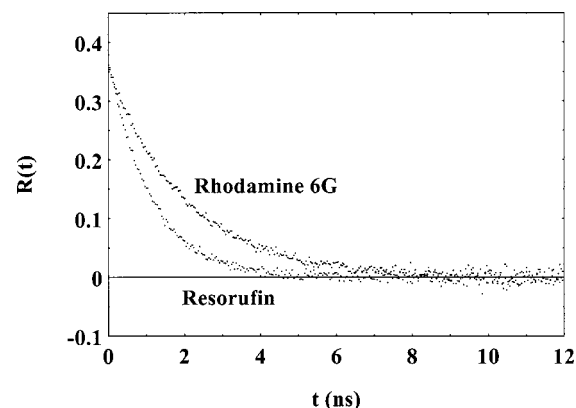

FIG. 2. Fluorescence anisotropy decays for rhodamine 6G and resorufin in isotropic ethylene glycol solutions. Isotropic rotational diffusion times of 2.15 and 1.2 ns are obtained which show intermediate behavior between stick and slip hydrodynamic boundary conditions.

TABLE I. Structural parameters and isotropic alignment relaxation times in ethylene glycol (at 25 °C) for rhodamine 6G and resorufin.

	V (Å^3)	Axial ratio	τ_{or} (ns)
Rhodamine 6G	416	0.286	2.15
Resorufin	165	2.4	1.2

III. EXPERIMENT

Free jets of rhodamine 6G and resorufin in ethylene glycol ($\approx 10^{-4}$ M) were produced from a precision 100 μm sapphire nozzle (Victor Kyburz AG) using a temperature controlled dye laser circulator (Coherent 5920). Stable laminar flows with Reynolds numbers in the region of 100 were attainable over a range of backing pressures and temperatures (20–30 psi and 17–30 °C) giving mean flow velocities spanning 2–3 ms^{-1}. As described earlier[1,2] we employ a 180° geometry as shown in Fig. 3 for the excitation and collection of molecular fluorescence from the jet, this together with a standard time correlated single photon counting (TCSPC) system with an instrument response function of 105 ps is used to obtain the $I_V(t)$ and $I_H(t)$ components of the fluorescence decay for a given excitation polarization angle β. An overall schematic of the apparatus is depicted in Fig. 4.

In conventional fluorescence polarization experiments on unaligned (isotropic) samples any polarization bias in the apparatus is often corrected for by tail matching of $I_V(t)$ and $I_H(t)$ decays which become equivalent as the molecules return to their isotropic equilibrium. The parameter obtained from such a measurement, the so-called system g-factor,[20,21] is then used in the subsequent determination of the fluorescence anisotropy $R(t)$. In the measurement of polarized fluorescence from aligned media in which the equilibrium excited state configuration is itself anisotropic it is crucial that the system g-factor is unity for the accurate determination of $R(t)$ from $I_V(t)$ and $I_H(t)$ decays. A g-factor of unity in our apparatus is evidenced by the equivalence of the $I_V(t)$ and $I_H(t)$ decays obtained from an isotropic sample using an excitation polarization angle of $\beta = 45°$,[1] the result of such a measurement is illustrated in Fig. 5.

The identification of the existence of an axis of cylindrical symmetry in a given sample is an important prerequisite for the implementation of the $R(t,\beta)$ measurements outlined in Paper I. This is most effectively achieved by the measurement of $R(t)$ as a function of the azimuthal jet angle ϕ m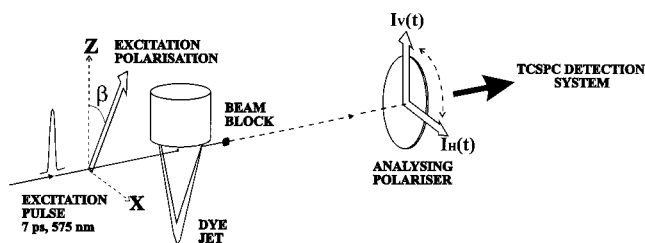easured perpendicular to the laboratory z axis for an excitation polarization angle of $\beta = 90°$ as illustrated in Fig. 6. This configuration ensures that the polarization vector of the excitation pulse is unaffected by reflection as ϕ is varied and that the effect of any cylindrical asymmetry on the fluorescence observables is maximized. The results of such measurements for the excitation of emerging dye molecules at
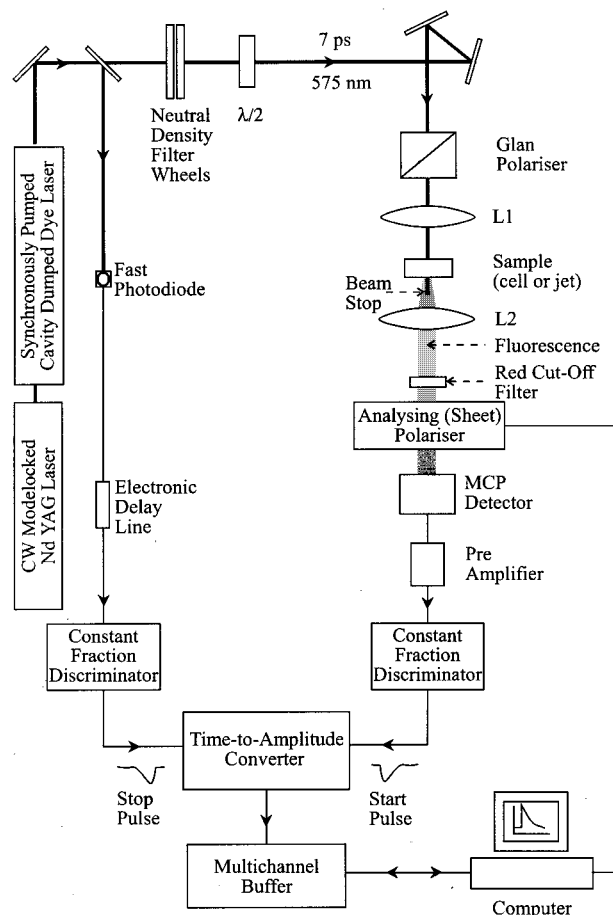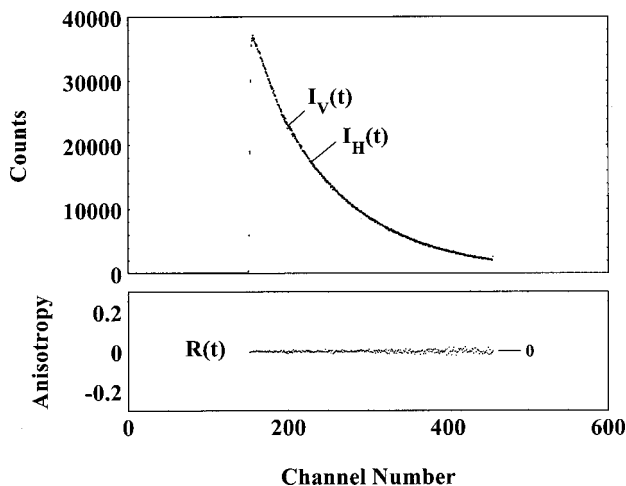

FIG. 4. The overall experimental arrangement showing the principal optical layout and the TCSPC system components.

FIG. 5. $I_V(t)$ and $I_H(t)$ decays obtained from an isotropic sample using an excitation polarization angle of $\beta = 45°$. Zero polarization bias in the detection system (a g-factor of unity) can be seen from the equivalence of the two signals yielding a time independent fluorescence anisotropy of zero.
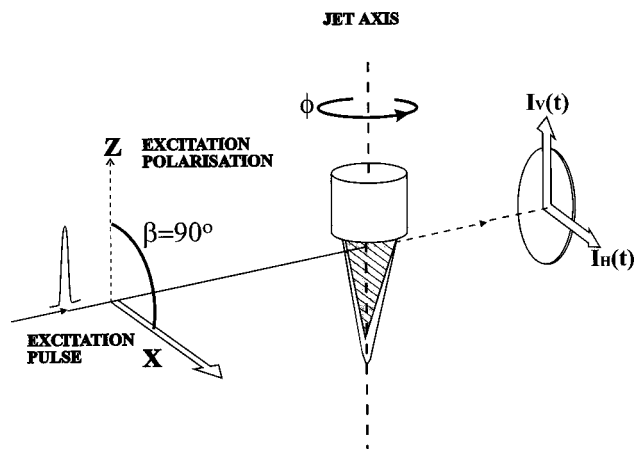

FIG. 3. A schematic of the 180° excitation-fluorescence detection geometry used in this work.

FIG. 6. A schematic of the experimental configuration employed to investigate the cylindrical symmetry of the molecular distributions in the jet. A P-polarized excitation pulse ($\beta=90°$) is employed, and with this arrangement the variation in the jet azimuth angle (ϕ) gives the greatest variation in the ϕ-dependent transition probability for this configuration. The use of this experimental arrangement also ensures that there is no depolarization of the excitation pulse due to the differential S and P reflectivities with ϕ at the jet surface.

the center of the nozzle exit and at the bottom of the jet in the region where the side lobes converge[22] are shown in Fig. 7. From this it is clear that an axis of cylindrical symmetry exists about the central flow direction at the nozzle exit of the jet but at the bottom of the jet a slight degree of cylindrical asymmetry has been imparted to dye molecules.

IV. STEADY-STATE ORDER MEASUREMENTS

Fluorescence anisotropy decays for rhodamine 6G and resorufin obtained in the nozzle exit region at $\approx 17\ °C$ with a pressure of 30 psi (mean flow velocity of $3\ \text{ms}^{-1}$) as a function of excitation polarization angle β with a laser spot size of approximately 50 μm, are shown in Fig. 8. As observed
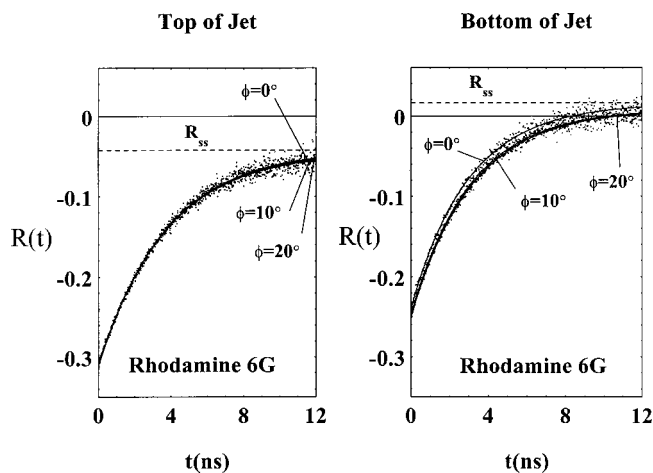

FIG. 7. (a) Fluorescence anisotropy decays recorded for rhodamine 6G and resorufin in the nozzle exit region for jet azimuthal angles of $\phi=0°$, 5°, 15°, 20°. To within experimental error the decays are identical indicating the presence of an axially symmetric ground state. (b) Fluorescence anisotropy decays recorded for rhodamine 6G and resorufin at the bottom of the jet for azimuthal angles of $\phi=0°-20°$. A distinct variation in the time dependent signals can be seen indicating the presence of cylindrical asymmetry with respect to the jet axis.
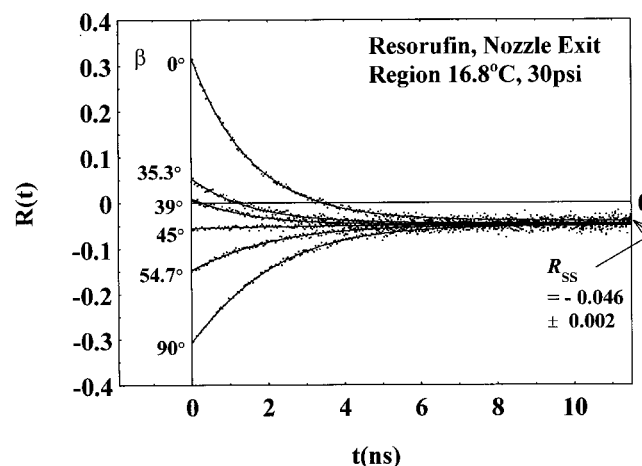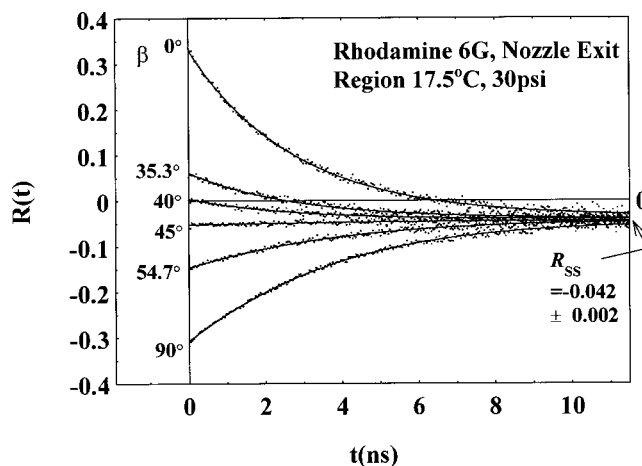

FIG. 8. Fluorescence anisotropy decays obtained in the nozzle exit region for resorufin and rhodamine 6G and resorufin as the excitation polarization angle β is varied from 0° to 90°.

previously, irrespective of the initial photoselection conditions the fluorescence anisotropy decays to a constant negative value R_{ss} consistent with a negative perpendicular alignment of both molecules in the flow.[1,2] From Fig. 8 it can be seen that an excitation polarization angle of $\beta=45°$ yields an effectively time independent fluorescence anisotropy equal to R_{ss}. It is thus possible to accurately assess the degree of steady state alignment in the jet from $R(t,\beta=45°)$ decays. Plots of R_{ss} along the jet axis as a function of downstream position from the nozzle exit for both systems are shown in Fig. 9. As can be seen the sign, magnitude, and spatial variation of R_{ss} for both molecules follows the same pattern, in the vicinity of the nozzle exit R_{ss} is in the region of -5% corresponding to a negative cylindrically symmetric alignment about the flow direction. This ordering of the emerging molecules persists for about 250 μs (assuming an average flow velocity of $3\ \text{ms}^{-1}$) before the onset of an isotropic region ($R_{ss}=0$) 0.75 mm downstream from the nozzle exit followed by establishment of a weak positive alignment ($R_{ss}<1\%$) at the bottom of the jet in agreement with our earlier observations.[1,2] This spatial dependence was found to be a common feature of both the rhodamine 6G and resorufin jets, the sign and magnitude of R_{ss} in the nozzle exit region
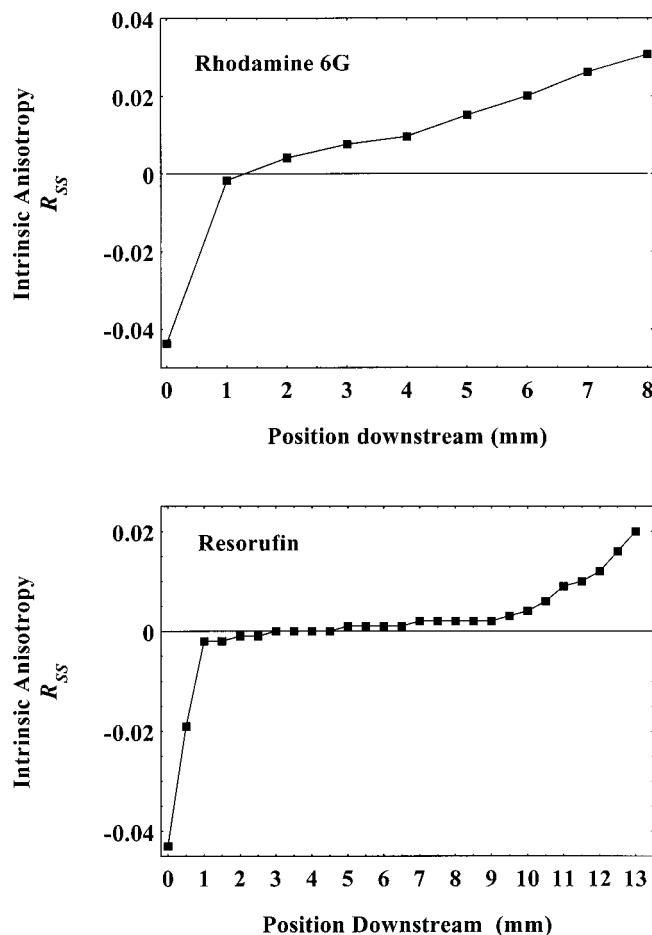
FIG. 9. The variation in the steady state anisotropy as a function of the downstream position from the nozzle exit.

TABLE II. Diffusion rates and asymmetry parameters for rhodamine 6G and resorufin together with the predicted degree of alignment expected for a shear rate of 1.2×10^5 s^{-1}.

	$4D=\dfrac{2}{3}\gamma_{20}(\text{s}^{-1})$	A	$\dfrac{\lambda A}{4D}$
Rhodamine 6G	3.6×10^8	0.88	2.9×10^{-4}
Resorufin	5.8×10^8	0.72	1.5×10^{-4}

showed little variation over the range of temperatures and flow velocities studied. The rotational motions of both rhodamine 6G and resorufin take place on a timescale significantly faster than changes in the jet due to fluid flow. The orientational dynamics measured by TCSPC at any given position in the jet represent the response of the solute molecules to an effectively static environment. The relationship between R_{ss} and the orientational energy in the flow measured relative to the flow axis is given by[1]

$$\ln\left[1+\frac{5}{2}R_{ss}(3\cos^2\theta-1)\right]=\frac{E(\theta=54.7°)-E(\theta)}{kT}. \quad (4.1)$$

The depth of the angle dependent potential is thus

$$\frac{E(\theta=0°)-E(\theta=90°)}{kT}=\ln\left[\frac{\left[1-\frac{5}{2}R_{ss}\right]}{1+5R_{ss}}\right]. \quad (4.2)$$

For $R_{ss}=-5\%$ an apparent well depth of 0.40 kT is indicated which is a significant degree of steady state alignment in comparison to that attainable for similar species using conventional flow or electric field alignment techniques. At this point it is instructive to consider the shear forces and velocity gradients that have the potential for producing molecular alignment in a high velocity fluid flow. The simplest case of confined fluid flow is that of laminar flow through a pipe, here the fluid layer that is adjacent to the (stationary) solid surface has zero velocity. The force acting to flow the fluid (tangential to the surface), creates a shear stress along the direction of the flow. For a pipe of radius a the velocity distribution of laminar flow is parabolic with a maximum velocity given by $v_{\max}=Pa^2/4\eta$, where P is the pressure gradient and η is the fluid viscosity. In the transition from confined to free fluid flow, the loss of the drag imposed by the walls and the boundary layer allows the outer fluid layers to increase in speed, leading to a constant velocity distribution across the jet. The nozzle used in this work has a rectangular cross section and gives rise to a triangular shaped free jet. The evolution of the jet shape arises from surface tension which, acting normally to the fluid surface, will minimize the free energy of the system by minimizing its surface area. For the initially ''flat'' jet that emerges from the sapphire nozzle this causes the edges to be drawn inward and to attain a circular cross section. The edges thicken with distance from the nozzle exit and become turbulent,[22] until finally merging. The triangular section between these edges remains interferometrically flat.[22,23] In Couette flow a linear shear of the form $\lambda=dv_Z/dX$ gives rise to the orientational distribution function in Eq. (2.3), the flow gradients operating in the nozzle and in the free jet will be considerably more complex. Nonetheless the molecular response to the shear should be expected to have a similar form to that of Eq. (2.3). Thus considering an average laminar flow of 3 ms^{-1} within the nozzle, the greatest shear forces will be experienced across the smallest dimension (Y) in the nozzle with a change in velocity from zero to 6 ms^{-1} occurring over the nozzle half thickness (50 μm). Assuming for simplicity that the shear is linear this yields a substantial value for λ of 1.2×10^5 s^{-1}. This is contrasted by the rapid orientational relaxation rates for resorufin and rhodamine 6G ($\approx10^8$ s^{-1}) which together with the relevant asymmetry factors are listed in Table II. From these data the maximum strength of the molecular response to the shear, given by $\lambda A/4D$, can be expected to be on the order of 10^{-4} for both resorufin and rhodamine 6G. Given shear forces of the appropriate symmetry this degree of molecular response would yield intrinsic anisotropies of less than 0.1%, well over two orders of magnitude less than the R_{ss} values of $\approx-5\%$ observed at the nozzle exit (Fig. 8). Couette alignment arises from the shear generated by the velocity gradients of the form dv_Z/dX and the torques so generated will give rise to a positive alignment of the long molecular axis of the solute in the flow direction.
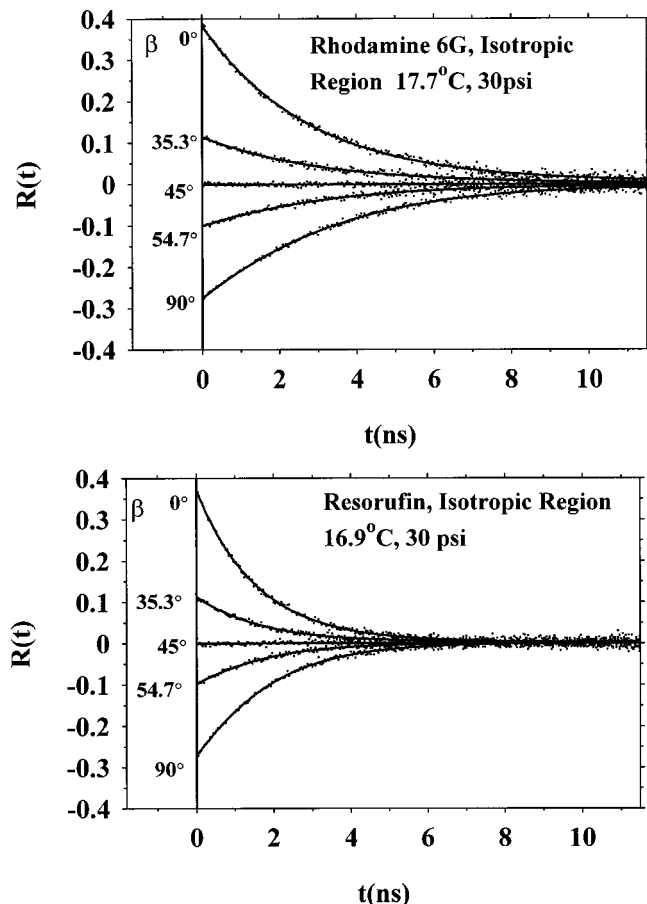
FIG. 10. Rhodamine 6G and resorufin $R(t,\beta)$ decays obtained at $\approx 3/4$ mm from the sapphire nozzle exit where the excited state alignment is zero. In this region the rotational diffusion dynamics are isotropic with $\gamma_{20} = \gamma_{22}$.
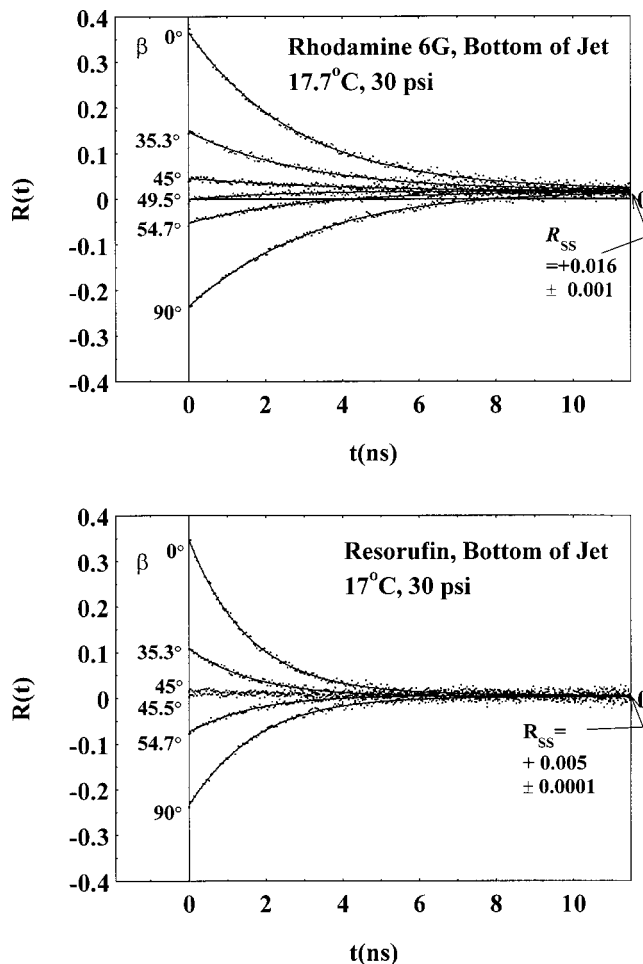

FIG. 11. Fluorescence anisotropy decays obtained at the bottom of the jet in the region immediately preceding the convergence of the lateral lobes of the flow. For both dye molecules a small positive steady state alignment is observed with $\gamma_{20} < \gamma_{22}$.

The relative magnitudes of the two shears would be expected to follow the X/Y aspect ratio of 7 mm to 100 μm with $dv_Z/dY = 70(dv_Z/dX)$. The loss of the boundary layer will significantly alter dv_Z/dY with dv_Z/dX little effected at the center of the flow. The asymmetry in the two torques presumably tends to zero downstream, and would not be expected to give rise to the cylindrically symmetric negative molecular alignment that is observed. The insensitivity of R_{ss} in this region to changes in the flow velocity (v_Z) is a further indication that alignment we observe is unlikely to originate from a Couette-type shear. In achieving fast flow rates there was an unavoidable rise in the jet temperature, this variation was however slight and changes to $k_B T$ over the whole temperature range (~ 17–$30\,°$C) are on the order of 3%, the absolute depth of the angle-dependent potential determined by Eq. (4.2) therefore shows little change with either v_Z or temperature. Shear forces arising from tangential velocity gradients of the form dv_X/dZ and dv_Y/dZ are however wholly compatible with the production of negative molecular alignment. The discontinuity in the flow caused by the removal of the liquid–sapphire interface may, until counteracted by surface tension, give rise to such gradients. The nature of fluid flow in the vicinity of a discontinuous boundary is not well understood, the forces generated may well be substantial and simple hydrodynamic models for the molecular response [e.g., Eq. (2.3)] under these conditions may not be applicable. Electric field alignment due to the frictional charging of the insulating sapphire surfaces by the fluid flow is perhaps an alternative mechanism, we have recently observed a change of several volts in the potential of the nozzle relative to ground as the jet is established.[24] The imposition of a potential at the boundary of an electrolytic solution will lead to the establishment of anion (resorufin) and cation (rhodamine 6G) concentration gradients at the interface, for a binary electrolyte the extent of these effects (even for significant surface charge densities) are characterized by Debye lengths in the range of 10^{-8} m with corresponding ion concentrations on the order of 10 M.[25] An increase in the concentration of molecules in the Debye region would be expected to lead [if significant in relation to the population in the bulk of the jet (≈ 100 μm)] to an increase in the measured fluorescence lifetime due to energy transfer and self-absorption.[26,27] This is not observed, as can be seen from Table III in the nozzle exit region there is a consistently lower fluorescence lifetime (between $\approx 2\%$–6%) relative to the isotropic region for both dye molecules. At present therefore the most likely mechanism for molecular alignment in the nozzle exit region would appear to lie with tangential shear forces arising from the transition from confined to free fluid flow.

TABLE III. Fluorescence lifetimes of rhodamine 6G and resorufin in the three regions of the jet. In both dyes there is an increase in the S_1 lifetime on passing from the region of negative steady state alignment at the nozzle exit to the main isotropic body of the fluid downstream.

	Rhodamine 6G τ_f (ns)	Resorufin τ_f (ns)
Nozzle exit region	4.59	4.69
Isotropic region	4.91	4.78
Bottom of jet	5.04	4.88

V. TIME-DEPENDENT FLUORESCENCE MEASUREMENTS

$R(t,\beta)$ decays for both rhodamine 6G and resorufin were measured at three points along the jet axis; first in the nozzle exit region (cylindrically symmetric negative steady state alignment), second in the isotropic region ≈ 1 mm downstream of the nozzle exit and finally at the bottom of the jet (slight positive alignment and cylindrical asymmetry). The results of these measurements are displayed in Figs. 8, 10, and 11, respectively.

Variation of the excitation polarization angle β with respect to the flow axis of the jet as shown in Fig. 3 yields an initial excited state distribution whose moments are given by Eq. (6.3) in Paper I,

$$\langle C_{KQ}^{\text{ex}}(0)\rangle = \frac{2C}{3}\sum_{K'Q'}\langle C_{K'Q'}^{gs}(ss)\rangle\left[\delta_{K'K}\delta_{Q'Q}\right.$$
$$+\frac{2}{\sqrt{5}}\sum_{Q''}d_{0-Q''}^2(-\beta)\begin{pmatrix}K & 2 & K'\\-Q & Q'' & Q'\end{pmatrix}$$
$$\times\left.\begin{pmatrix}K & 2 & K'\\0 & 0 & 0\end{pmatrix}\sqrt{5}\hat{K}\hat{K}'\right]. \tag{5.1}$$

For an axially symmetric ground state $Q'=0$ and the initial fluorescence anisotropy is thus sensitive to the cylindrically symmetric alignment and hexadecapole moments according to Eq. (6.10) in Paper I. Plots of the initial anisotropy $R(0,\beta)$ can in principle be used to determine the ground state distribution function. Before this is done it is necessary to con-

sider the factors which can cause a reduction in the measured anisotropy from its true value. These include the finite time resolution of the TCSPC system, the possible (small) non-parallelism of the absorption and emission transition dipole moments and depolarization of the fluorescence by the optical components of the analyzing system or by self-absorption. The reduction in the value of $R(0,\beta=0°)$ from 0.4 is typically in the region of 0.95 and 0.96 for rhodamine 6G and resorufin, respectively. Approximating the instrument response to a Gaussian with a full width ≈ 100 ps the reduction in $R(0,\beta=0°)$ is expected to be on the order of 0.5% for both dyes, only when this is increased to ≈ 400 ps—well above the measured response time—does the expected reduction in $R(0,\beta=0°)$ agree with that observed. A rotation of the transition moment direction through an angle γ in the molecular frame gives rise to a modification of the initial moments $\langle C_{KQ}^{\text{ex}}(0)\rangle$ of the excited state distribution by a factor $P_K(\cos\gamma)$.[16] An angle of $\gamma=15°$ would be necessary to account for the measured reduction in $R(0,\beta=0°)$, however this would be expected to lead to a nonsingle exponential decay in $R(t,\beta=0°)$ which is not observed in this or other studies.[19,20] The existence of a single exponential isotropic anisotropy decay in a symmetric rotor such as resorufin is generally accepted as evidence that $\gamma=0°$.[28] The reduction in $R(0,\beta=0°)$ with increasing concentration and path length is well known[21] as is the depolarization of fluorescence by the collection optics.[29] It is the combination of these two factors that is the most likely cause for the small reductions in $R(0,\beta)$ that are observed. The effect of all the above factors is to modify the alignment components from their true values by an amount parameter $\bar{A}$, and with this modification $R(0,\beta)$ becomes

$$R(0,\beta)=\frac{\left[\frac{2}{5}(\cos^2\beta-\sin^2\beta)+\right]\bar{A}}{1+\bar{A}\frac{2}{5}\sin^2\beta}. \tag{5.2}$$

For rhodamine 6G and resorufin values for $\bar{A}$ of 0.95 and 0.97 were determined from fits to the $R(0,\beta)$ data using Eq. (5.2). In a similar manner the initial anisotropy in the nozzle exit region [Paper I, Eqs. (3.12) and (6.7)–(6.9)] becomes

$$R(0,\beta)=\frac{\left[\frac{2}{5}(\cos^2\beta-\sin^2\beta)+\frac{\langle\alpha_{20}^{gs}(ss)\rangle}{\sqrt{5}}\left[1+\frac{4}{7}\cos^2\beta\right]+\frac{\langle\alpha_{40}^{gs}(ss)\rangle}{35}(19\cos^2\beta-7)\right]\bar{A}}{1+\bar{A}\frac{2}{5}\sin^2\beta+\frac{\langle\alpha_{20}^{gs}(ss)\rangle}{\sqrt{5}}\left[\frac{(21-4\bar{A})\cos^2\beta-(7+4\bar{A})}{7}\right]+\frac{\langle\alpha_{40}^{gs}(ss)\rangle}{35}2\bar{A}\sin^2\beta}. \tag{5.3}$$

Fits to $R(0,\beta)$ for both dye molecules in the nozzle exit region are shown in Fig. 12 and indicate that to within experimental error the degree of steady state alignment in the ground and excited states are equal and the contribution from

higher ground state moments ($\langle\alpha_{40}^{gs}(ss)\rangle$) is negligible. From this information it is reasonable to assume that both equilibrium distribution functions correspond well to that of a purely aligned array,

$$P(\theta,\phi(ss)) = \frac{1}{4\pi}\left[1 + \langle\alpha_{20}(ss)\rangle\frac{1}{2}(3\cos^2\theta - 1)\right]. \qquad (5.4)$$

An additional experimental parameter of use here is the sample magic angle β_M, the excitation polarization angle for which the initial anisotropy is zero. For a purely aligned ground state the sample magic angle was shown to be [Paper I, Eq. (6.11)]

$$\cos^2\beta_M = \frac{14 - \dfrac{35\langle\alpha_{20}^{gs}(ss)\rangle}{\sqrt{5}}}{28 + \dfrac{20\langle\alpha_{20}^{gs}(ss)\rangle}{\sqrt{5}}}. \qquad (5.5)$$

In the nozzle exit region β_M values of 39° and 40° were recorded for resorufin and rhodamine 6G, respectively. Predictions based on the ground state alignment values calculated from the $R(0,\beta)$ data give corresponding β_M values of 39.5° and 40.1°. The uncertainty in $\langle\alpha_{20}^{gs}(ss)\rangle/\sqrt{5}$ should be no greater than that for R_{ss} which gives an angular error in β_M of $\pm2°$, there is therefore excellent agreement between experiment and theory.

VI. ALIGNMENT DYNAMICS

From Paper I it was found that to first order the anisotropic diffusion dynamics of the excited state alignment in the nozzle exit region should have the form,

$$\langle\alpha_{20}^{ex}(t)\rangle = \langle\alpha_{20}^{ex}(ss)\rangle + \{\langle\alpha_{20}^{ex}(0)\rangle - \langle\alpha_{20}^{ex}(ss)\rangle\}\exp(-\gamma_{20}t)$$

$$\{\langle\alpha_{22}^{ex}(t)\rangle + \langle\alpha_{2-2}^{ex}(t)\rangle\} = \{\langle\alpha_{22}^{ex}(0)\rangle + \langle\alpha_{2-2}^{ex}(0)\rangle\}$$
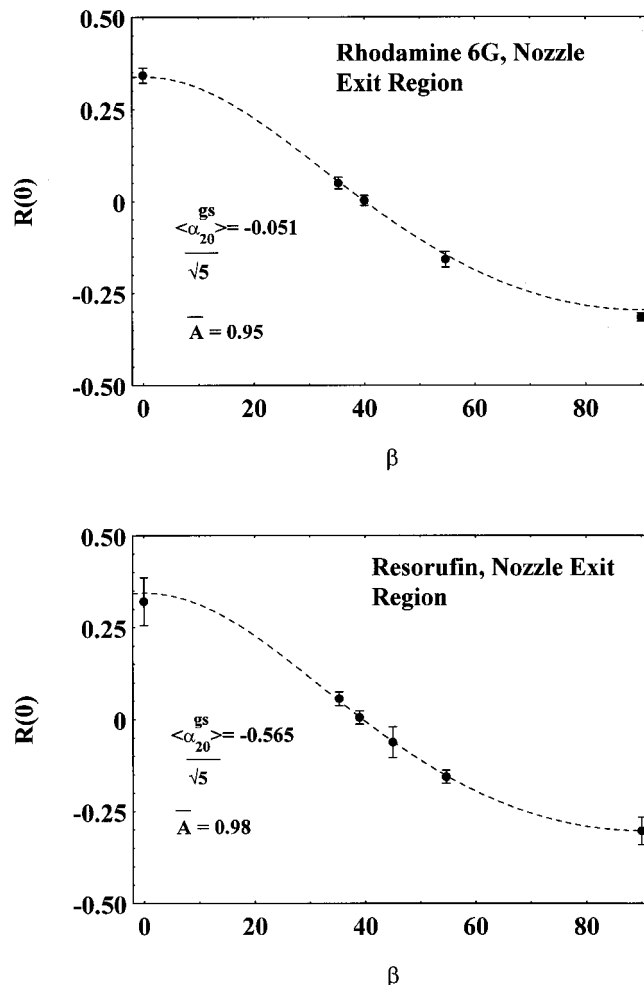$$\times\exp(-\gamma_{22}t), \qquad (6.1)$$

FIG. 12. Variation in the initial fluorescence anisotropy with excitation polarization at the nozzle exit. Fits to the data using Eq. (5.3) are shown by the dashed line and indicate that the ground state anisotropy is characterized solely by the cylindrically symmetric alignment $\langle\alpha_{20}\rangle$. The data also indicate a small degree of depolarization of the fluorescence by the system optics (2%–5%).

where γ_{20} and γ_{22} represent the pure θ diffusion and the θ plus ϕ diffusion rates, respectively (see Paper I, Sec. VI). The variation in $R(t)$ with the excitation polarization angle β in an intrinsically aligned medium with axial symmetry assuming and allowing for the net depolarization of the signal ($\bar{A}\langle1$) is given by [Paper I, Eq. (7.8)],

$$R(t,\beta) = \frac{\left[\begin{array}{l}\left[(3\cos^2\beta-1)\left[\dfrac{1}{5} + \dfrac{\langle\alpha_{20}^{gs}(ss)\rangle}{\sqrt{5}}\left[\dfrac{2}{7} - \dfrac{\langle\alpha_{20}^{ex}(ss)\rangle}{\sqrt{5}}\right]\right] + \left\{\dfrac{\langle\alpha_{20}^{gs}(ss)\rangle - \langle\alpha_{20}^{ex}(ss)\rangle}{\sqrt{5}}\right\}\right]\exp(-\gamma_{20}t)\\ -\dfrac{\sin^2\beta}{5}\left[1 - \dfrac{10\langle\alpha_{20}^{gs}(ss)\rangle}{7\sqrt{5}}\right]\exp(-\gamma_{22}t) + \left\{\dfrac{\langle\alpha_{20}^{ex}(ss)\rangle}{\sqrt{5}}\right\}\left(1 + (3\cos^2\beta-1)\dfrac{\langle\alpha_{20}^{gs}(ss)\rangle}{\sqrt{5}}\right)\end{array}\right]}{\dfrac{1}{\bar{A}}\left[1 + (3\cos^2\beta-1)\dfrac{\langle\alpha_{20}^{gs}(ss)\rangle}{\sqrt{5}}\right] + \dfrac{2}{5}\sin^2\beta\left[1 - \dfrac{10}{7}\dfrac{\langle\alpha_{20}^{gs}(ss)\rangle}{\sqrt{5}}\right]\exp(-\gamma_{22}t)}. \qquad (6.2)$$

Since the ground and excited state equilibrium degrees of alignment are equal ($\langle\alpha_{20}^{ex}(ss)\rangle/\sqrt{5} \cong \langle\alpha_{20}^{gs}(ss)\rangle/\sqrt{5} = R_{ss}$), Eq. (6.2) simplifies to

$$R(t,\beta)=\frac{\left[\begin{array}{l}\left[\left[(3\cos^2\beta-1)\left[\frac{1}{5}+R_{ss}\left[\frac{2}{7}-R_{ss}\right]\right]\right]\exp(-\gamma_{20}t)\right.\\\left.-\frac{\sin^2\beta}{5}\left[1-\frac{10}{7}R_{ss}\right]\exp(-\gamma_{22}t)+R_{ss}(1+(3\cos^2\beta-1)R_{ss})\right.\end{array}\right]}{\frac{1}{A}[1+(3\cos^2\beta-1)R_{ss}]+\frac{2}{5}\sin^2\beta\left[1-\frac{10}{7}R_{ss}\right]\exp(-\gamma_{22}t)}. \tag{6.3}$$

The anisotropy decay in these circumstances should therefore follow

$$R(t,\beta)=\frac{A(\beta)\exp(-\gamma_{20}t)-B(\beta)\exp(-\gamma_{22}t)+C}{\frac{1}{A}+2B(\beta)\exp(-\gamma_{22}t)}, \tag{6.4}$$

where

$$A(\beta)=\frac{A_{20}(\beta)}{N(\beta)}=\left[(3\cos^2\beta-1)\left[\frac{1}{5}+R_{ss}\left[\frac{2}{7}-R_{ss}\right]\right]\right]\bigg/[1+(3\cos^2\beta-1)R_{ss}],$$

$$B(\beta)=\frac{A_{22}(\beta)}{N(\beta)}\frac{\sin^2\beta}{5}\left[1-\frac{10}{7}R_{ss}\right]\bigg/[1+(3\cos^2\beta-1)R_{ss}], \tag{6.5}$$

$$C=R_{ss}.$$

In the case of cylindrical asymmetry as pertains to the bottom of the jet both alignment moments can be expected (neglecting cross relaxation) to decay to steady state values along the lines of Eq. (5.3). The form of the anisotropy decay in these circumstances will follow,

$$R(t,\beta)=\frac{\left[\begin{array}{l}\frac{1}{\sqrt{5}}[[\langle C_{20}^{ex}(0,\beta)\rangle-\langle C_{20}^{ex}(ss)\rangle]\exp(-\gamma_{20}t)+\langle C_{20}^{ex}(ss)\rangle]\\-\frac{1}{\sqrt{30}}[[\{\langle C_{22}^{ex}(0,\beta)\rangle+\langle C_{2-2}^{ex}(0,\beta)\rangle\}-\{\langle C_{22}^{ex}(ss)\rangle+\langle C_{2-2}^{ex}(ss)\rangle\}]\exp(-\gamma_{22}t)+\{\langle C_{22}^{ex}(ss)\rangle+\langle C_{2-2}^{ex}(ss)\rangle\}]\end{array}\right]}{\langle C_{00}^{ex}(0,\beta)\rangle+\frac{2}{\sqrt{30}}\left[\begin{array}{l}[\{\langle C_{22}^{ex}(0,\beta)\rangle+\langle C_{2-2}^{ex}(0,\beta)\rangle\}-\{\langle C_{22}^{ex}(ss)\rangle+\langle C_{2-2}^{ex}(ss)\rangle\}]\exp(-\gamma_{22}t)\\+\{\langle C_{22}^{ex}(ss)\rangle+\langle C_{2-2}^{ex}(ss)\rangle\}\end{array}\right]}, \tag{6.6}$$

the general form of which will be

$$R(t,\beta)=\frac{A'(\beta)\exp(-\gamma_{20}t)-B'(\beta)\exp(-\gamma_{22}t)+[A(ss)-B(ss)]C'(\beta)}{C'(\beta)+2B'(\beta)\exp(-\gamma_{22}t)+2B(ss)C'(\beta)}, \tag{6.7}$$

where $A'(\beta)$, $B'(\beta)$, and $C'(\beta)$ are parameters which depend on the initial photoselection and the ground state anisotropy [Paper I, Eqs. (6.4)–(6.6)] and $[A(ss)-B(ss)]/1+2B(ss)=R_{ss}$. In the case of weak cylindrical asymmetry at the bottom of the jet the β-dependent terms should not show a significant departure from those obtained for excitation from a weak positively aligned ground state [i.e., Eqs. (6.4) and (6.5) with R_{ss} positive].

In the nozzle exit region the analysis of the $R(t,\beta)$ decays was undertaken as follows: γ_{20} was determined from a least squares fit to the $\beta=0°$ decay using Eq. (6.4) yielding a single exponential decay of the form,

$$R(t,\beta=0°)=(A(\beta)\exp(-\gamma_{20}t)+C)\bar{A}. \tag{6.8}$$

As the ground and excited state degrees of alignment are the

same the $\beta=54.7°$ decay is dominated by the asymmetric alignment dynamics, a similar procedure was followed to determine γ_{22} giving a decay of the form,

$$R(t,\beta)=\frac{C-B(\beta)\exp(-\gamma_{22}t)}{\frac{1}{A}+2B(\beta)\exp(-\gamma_{22}t)}. \tag{6.9}$$

The values γ_{20} and γ_{22} obtained in this way were then used as fixed parameters in a least squares fit to the $\beta=90°$ and all intermediate decays. In all of the fits $A(\beta)$, $B(\beta)$, and C were allowed to float but were constrained to have the appropriate sign as predicted by Eq. (6.5). The pre-exponential factors yielded by this process are in good agreement with the theoretical values as predicted by Eq. (6.5), as can be seen, for example, in Fig. 13 which shows the time zero pre-exponential factors obtained from fits to the $R(0,\beta)$ data and those obtained from the fits to the $R(t,\beta)$ decays for
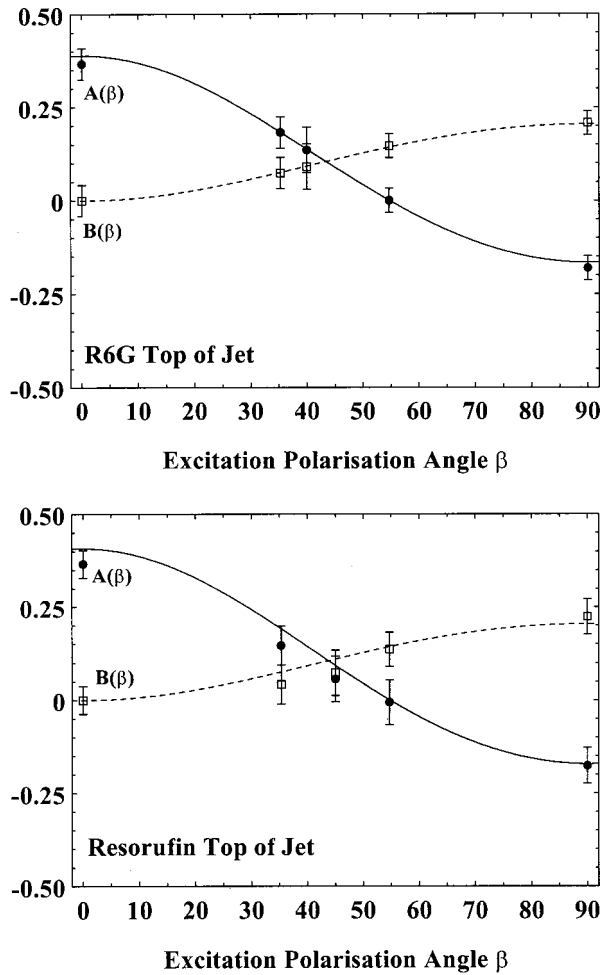
FIG. 13. Plots of the pre-exponential cylindrically symmetric $[A(\beta)]$ and asymmetric $[B(\beta)]$ degrees of alignment obtained from the nozzle exit $R(t,\beta)$ decays for rhodamine 6G and resorufin. Also shown are the theoretical predictions for $A(\beta)$ and $B(\beta)$ based on perturbed relaxation in a cylindrically symmetric medium as given by Eq. (6.4).

resorufin and rhodamine 6G. A similar procedure was followed in both the isotropic region and at the bottom of the jet where Eq. (6.8) is used as the fitting equation. In both regions of steady state molecular alignment the fits obtained for both dyes were in good agreement with the theoretical predictions of perturbed but linear orientational relaxation.

The γ_{20} and γ_{22} relaxation rates obtained for rhodamine 6G and resorufin are displayed in Table IV. The presence of a net molecular alignment whether positive or negative is seen to raise the γ_{20}/γ_{22} degeneracy. In the nozzle exit region with a negative cylindrically symmetric alignment γ_{20} is greater than γ_{22} for both molecules, whilst at the bottom of the jet (R_{ss} positive) this relationship is reversed. In the isotropic region γ_{20} and γ_{22} are equal consistent with isotropic rotational diffusion dynamics. From Table IV it can be seen that γ_{20} remains constant (to within experimental error) whilst γ_{22} shows significant variation as a function of the downstream position in the jet. At this point it is instructive to consider the sensitivity of γ_{20} and γ_{22} to external perturbations. General symmetry considerations developed in Paper I showed a perturbation of quadrupolar symmetry that

had equal but opposing effects on the two decays [Eq. (6.15)],

$$\gamma_{20}=6D'+\langle a_{20}\rangle\sqrt{\frac{2}{7}}\langle 2\|H^2\|2\rangle,$$

$$\gamma_{22}=6D'-\langle a_{20}\rangle\sqrt{\frac{2}{7}}\langle 2\|H^2\|2\rangle. \tag{6.10}$$

This result assumed that the deviation from isotropic relaxation dynamics occurred as the result of the imposition of an external force (e.g., an electric field) and that the global viscosity of the medium itself was unaffected. The general expression for γ_{KQ} is given by [Paper I, Eq. (7.10)]

$$\gamma_{KQ}=-\langle KQ|D\nabla^2+H'|KQ\rangle. \tag{6.11}$$

The diffusion operator $D\nabla^2$ can be written as

$$D\nabla^2=D_{XX}\hat{J}_X^2+D_{YY}\hat{J}_{YY}^2+D_{ZZ}\hat{J}_{ZZ}^2, \tag{6.12}$$

where D_{XX}, D_{YY}, and D_{ZZ} are the diagonal components of the diffusion tensor in the laboratory axis system. In an isotropic medium these three quantities are necessarily equal but in an anisotropic flowing fluid this requirement is lifted. In the nozzle exit region axial symmetry requires $D_{XX}=D_{YY}$, and under these circumstances the γ_{KQ} decay rates are given by

$$\gamma_{KQ}=-\langle KQ|D\nabla^2+H'|KQ\rangle \tag{6.13}$$

which on inserting Eq. (6.12) gives

$$\gamma_{KQ}=D_\perp[K(K+1)-Q^2]+D_\|Q^2+\langle KQ|H'|KQ\rangle, \tag{6.14}$$

where $D_{XX}=D_{YY}\equiv D_\perp$ and $D_{ZZ}\equiv D_\|$. In terms of an expansion of H' in isotropic and quadrupolar components [Paper I, Eq. (7.14)]

$$\gamma_{KQ}=D_\perp[K(K+1)-Q^2]+D_\|Q^2-\Big[\langle a_{00}\rangle\langle K\|H^0\|K\rangle$$

$$+\langle a_{20}\rangle\frac{3Q^2-K(K+1)}{\sqrt{K(K+1)(2K+3)(2K-1)}}\langle K\|H^2\|K\rangle\Big]. \tag{6.15}$$

For γ_{20} and γ_{22} this yields

$$\gamma_{20}=6D_\perp-\Big[\langle a_{00}\rangle\langle 2\|H^0\|2\rangle-\langle a_{20}\rangle\sqrt{\frac{2}{7}}\langle K\|H^2\|K\rangle\Big], \tag{6.16}$$

$$\gamma_{22}=2D_\perp+4D_\|-\Big[\langle a_{00}\rangle\langle 2\|H^0\|2\rangle+\langle a_{20}\rangle\sqrt{\frac{2}{7}}\langle K\|H^2\|K\rangle\Big]. \tag{6.17}$$

As can be seen from Table IV for given flow conditions γ_{20} remains approximately constant whilst γ_{22} shows significant variation between each of the three regions of the jet. Since $\langle KQ|D\nabla^2|KQ\rangle\gg\langle KQ|H'|KQ\rangle$ it is reasonable to assume that the variations γ_{22} arise primarily from differences in $D_\|$ as $\langle KQ|H'|KQ\rangle$ will necessarily vary with the degree of steady state alignment. This is further supported by the exact solution to the Debye equation for diffusion in a quadrupolar

TABLE IV. The variation in the cylindrically symmetric and asymmetric alignment dynamics for rhodamine 6G and resorufin in the three regions of the jet (see Figs. 8, 10, and 11). The intrinsic θ and ϕ diffusion rates are obtained from γ_{20} and γ_{22} using Eq. (6.23) and used to construct the diffusion anisotropy ratio A [Eq. (6.22)]. In the case of resorufin measurements of these quantities were obtained for a number of flow conditions yielding average jet velocities $\bar{v}$ in the range 2.4–3 ms^{-1}.

Rhodamine 6G	Temp (°C)	Pressure (psi)	$\bar{v}$(ms^{-1})	$\gamma_{20}\times10^9$ (s^{-1})	$\gamma_{22}\times10^9$ (s^{-1})	$D_\perp\times10^8$ (s^{-1})	$D_\perp\times10^8$ (s^{-1})	A	$R_{ss\%}$
Nozzle exit region	17.4	30	2.55	0.36	0.31	0.6	0.475	0.792	−4.2
Isotropic region	17.7	30	2.59	0.36	0.36	0.6	0.6	1	0
Bottom of jet	17.7	30	2.59	0.35	0.38	0.583	0.658	1.128	1.6
Resorufin									
Nozzle exit region	16.8	30	2.45	0.65	0.56	1.083	0.858	0.792	−4.6
Nozzle exit region	20	30	2.95	0.85	0.79	1.417	1.267	0.894	−5.2
Nozzle exit region	27	15	2.42	1.225	1.038	2.042	0.221	0.771	−4.6
Isotropic region	16.9	30	2.46	0.64	0.65	1.067	1.092	1.023	0
Bottom of jet	17	30	2.48	0.64	0.69	1.067	1.192	1.117	0.5
Bottom of jet	27.1	15	2.43	1.15	1.27	1.917	2.217	1.156	1.1

potential.[30] In the absence of anisotropic viscosity a significant variation in *both* γ_{20} and γ_{22} with the equilibrium order (in our case R_{ss}) is predicted. For a purely aligned system as found in the nozzle exit region this yields

$$\gamma_{20}=6D\left[\frac{7+R_{ss}}{7+5R_{ss}[2-7R_{ss}]}\right] \quad \text{and} \quad \gamma_{22}=6D\left[\frac{7-5R_{ss}}{7-10R_{ss}}\right].$$
(6.18)

While predicting the correct ordering of γ_{20} and γ_{22} at the immediate nozzle exit (6.18) does not account for the observed invariance in γ_{20} with increasing downstream position. It is therefore reasonable to conclude that the relaxation dynamics in the jet are dominated by anisotropic diffusion ($\langle KQ|D\nabla^2|KQ\rangle \gg \langle KQ|H'|KQ\rangle$). In this light the relationship between the θ and ϕ sensitivities of γ_{20} and γ_{22} derived in Paper I [Eq. (5.15)] are wholly applicable

$$\gamma_{22}=\frac{\gamma_{20}}{3}+\gamma_{22}(\phi),$$
(6.19)

where

$$\gamma_{22}(\phi)=4D_\parallel \quad \text{and} \quad \gamma_{20}=6D_\perp.$$
(6.20)

$D_\parallel$ and $D_\perp$ can therefore be obtained from

$$D_\parallel=\frac{1}{4}\left(\gamma_{22}-\frac{\gamma_{20}}{3}\right) \quad \text{and} \quad D_\perp=\frac{\gamma_{20}}{6}.$$
(6.21)

The diffusion anisotropy A [Paper I, Eq. (5.16)] is therefore

$$A=\frac{D_\parallel}{D_\perp}=\frac{1}{2}\left[3\frac{\gamma_{22}}{\gamma_{20}}-1\right].$$
(6.22)

Values of the diffusion anisotropy A in the three regions of the jet for both rhodamine 6G and resorufin together with the intrinsic θ and ϕ diffusion rates $D_\perp$ and $D_\parallel$ are also displayed in Table IV. Similar trends in orientational relaxation can be seen for both dye molecules; in the nozzle exit region a negative steady state alignment is seen to correspond to an intrinsic ϕ diffusion rate that is between approximately

79%–89% of the value for θ motion. For a steady state anisotropy of zero θ and ϕ diffusion rates are (to within experimental error) equivalent as is physically consistent with isotropic rotational diffusion. In the transition from a negative steady state alignment to an isotropic distribution of dye molecules there an increase of 70%–75% in γ_ϕ ($D_\parallel$) over that observed in the nozzle exit region. A further although less marked increase in γ_ϕ takes place with increasing positive jet alignment yielding a diffusion anisotropy A of ≈1.13–1.16.

The isotropic orientational dynamics of both rhodamine 6G and resorufin are well described by the Stokes–Einstein–Debye (SED) equation in the limit of slip hydrodynamics, where the observed diffusion coefficients have the form[18]

$$D=\frac{kT}{\eta VfC}.$$
(6.23)

Here, η is the solvent viscosity, V is the hydrodynamic molecular volume, f is the molecular shape factor, and C is a shape dependent parameter that accounts for the solvent–solute boundary conditions (for slip hydrodynamics $C<1$). Changes in molecular shape (i.e., altering V, f, and C) as a result of transport are well known in macromolecules[31,32] but are unlikely to occur in small rigid molecules. This is born out by the insensitivity of γ_{20} and γ_{22} to the initial photoselection (i.e., molecular orientation in the flow) and the retention of single exponential alignment dynamics in the case of rhodamine 6G where the orientational dynamics are sensitive to rotational diffusion parallel and perpendicular to the symmetry axis of the rotor. Applying Eq. (5.28) to the determination of A implies that for $\gamma_{20}\neq\gamma_{22}$ the viscosity of the solvent is necessarily anisotropic,

$$A=\frac{D_\parallel}{D_\perp}=\frac{1}{2}\left[3\frac{\gamma_{22}}{\gamma_{20}}-1\right]=\frac{\eta_\perp}{\eta_\parallel}.$$
(6.24)

The diffusion anisotropy can therefore be taken as a direct measure of the different solvent frictional forces for θ and ϕ
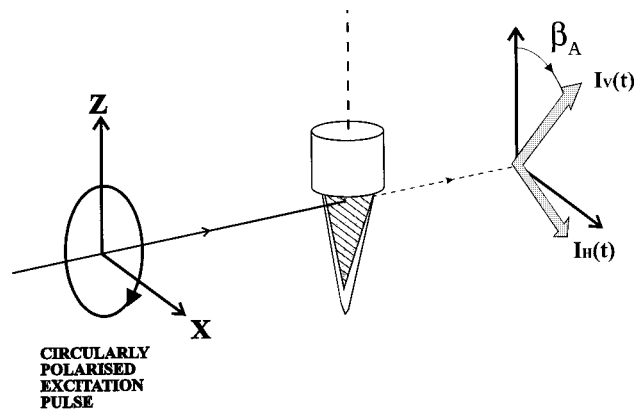
FIG. 14. A schematic representation of the experimental arrangement for circularly polarized excitation with collinear fluorescence anisotropy measurements defined in a rotated analyzer axis system with angle β_A to the flow axis of the jet.
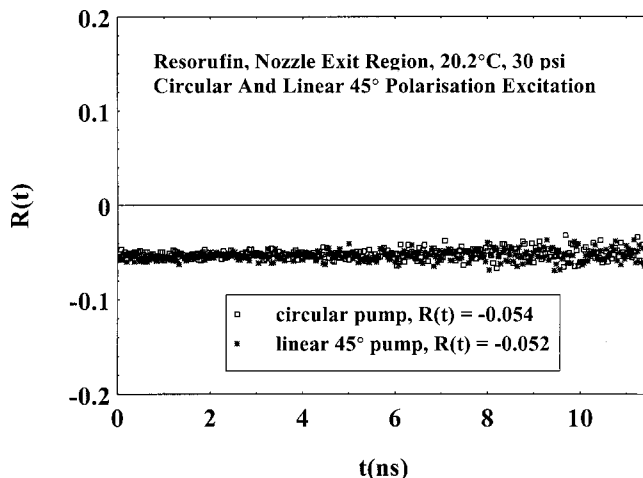

FIG. 15. Fluorescence anisotropy decays recorded in the nozzle exit region for resorufin with linearly polarized excitation at $\beta=45°$ and circularly polarized excitation with $\beta_A=0°$. The equivalence of the two signals is unequivocal evidence of the cylindrical symmetry of the molecular distribution in this region.

motion in the laboratory axis. Anisotropy in the bulk viscosity of an aligned medium is well known, for example, in the case of liquid crystals.[33] In the jet θ diffusion shows little deviation from isotropic behavior and it should be stressed that conventional fluorescence anisotropy experiments [$R(t,\beta=0°)$ measurements] which in general are sensitive solely to θ diffusion would not reveal this information.

VII. CIRCULARLY POLARIZED EXCITATION

Circularly polarized excitation provides a transition probability that is fundamentally different to excitation with a variable angle of linear polarization in that photoselection is isotropic in the plane perpendicular to the propagation direction of the excitation pulse. It was shown in Paper I that the equivalence of conventionally measured $R(t)$ signals obtained using circular and $\beta=45°$ linear excitation polarizations was unequivocal evidence for an axially symmetric ground state. Furthermore, as the transition probability contains no $Y_{2\pm1}(\theta,\phi)$ terms it was shown how the measurement of the subsequent fluorescence anisotropy in a sequence of rotated analyzer settings as illustrated in Fig. 14 was sensitive to the presence of the excited state $\langle C_{2\pm1}^{ex}\rangle$

moments, the observation of which is precluded in a conventional anisotropy measurement.

Figure 15 shows a comparison between $R(t,\beta=45°)$ and the corresponding anisotropy signal obtained for circularly polarized excitation of resorufin in the nozzle exit region. Both signals are essentially time independent and (within experimental error) wholly equivalent; this further confirms the axial symmetry of the dye molecules at the nozzle exit as indicated by the ϕ-dependent excitation measurements of Sec. II. In the laboratory axis system the circularly polarized excitation probability has the form [Paper I, Eq. (8.4)]

$$W_{abs}^{lab}(\theta,\phi,t)=BI(t)\frac{\sqrt{4\pi}}{3}\left[Y_{00}(\theta,\phi)+\frac{1}{\sqrt{20}}Y_{20}(\theta,\phi)\right.$$
$$\left.+\sqrt{\frac{3}{40}}\{Y_{22}(\theta,\phi)+Y_{2-2}(\theta,\phi)\}\right]. \quad (7.1)$$

The subsequent fluorescence anisotropy measured in the rotated analyzer axis system is given by [Paper I, Eq. (8.11)]

$$R(\beta_A,t)=\frac{(\cos^2\beta_A-\sin^2\beta_A)R(\sigma,\beta_A=0°,t)+2C(t)\sin\beta_A\cos\beta_A}{1+R(\sigma,\beta_A=0°,t)\sin^2\beta_A-C(t)\sin\beta_A\cos\beta_A}, \quad (7.2)$$

with

$$C(t)=\frac{2\{\langle\alpha_{21}^{ex}(t)\rangle-\langle\alpha_{2-1}^{ex}(t)\rangle\}}{\sqrt{30}+2\{\langle\alpha_{22}^{ex}(t)\rangle+\langle\alpha_{2-2}^{ex}(t)\rangle\}}. \quad (7.3)$$

In an axially symmetric medium circularly polarized excitation is unable to create $\langle\alpha_{21}^{ex}\rangle$ or $\langle\alpha_{2-1}^{ex}\rangle$, and $C(t)$ in the nozzle exit region is therefore zero and Eq. (7.2) becomes

$$R(\beta_A,t)=\frac{(\cos^2\beta_A-\sin^2\beta_A)R(\beta_A=0°,t)}{1+R(\beta_A=0°,t)\sin^2\beta_A}. \quad (7.4)$$

Measurements of the fluorescence anisotropy following circularly polarized excitation were performed for a range of analyzer settings (β_A) from 0° to 90° for rhodamine 6G and resorufin in the nozzle exit region the results of which are displayed in Fig. 16. The fluorescence anisotropy for a given value of β_A shows no measurable time dependence. The av-
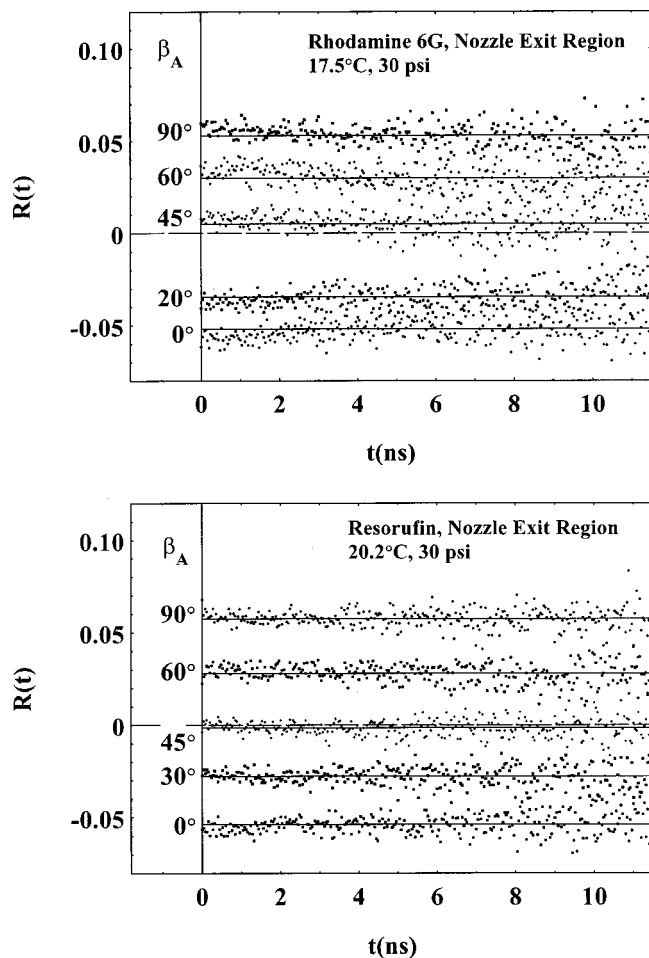
FIG. 16. Circularly polarized fluorescence anisotropy signals recorded in the nozzle exit region for varying values of β_A. The time independence of the data is consistent with isotropic photoexcitation in the $z-x$ plane to an excited state whose alignment is equal to that of the ground state.

FIG. 17. Fits to the time independent $R(t,\beta_A)$ signals obtained in the nozzle exit region of the jet (Fig. 16) using Eq. (7.2). The results are consistent with an excited state in which the $\langle \alpha_{20}^{ex} \rangle$ and $\{\langle \alpha_{22}^{ex} \rangle + \langle \alpha_{22}^{ex} \rangle\}$ alignment terms are at or close to their steady state values with no $\{\langle \alpha_{21}^{ex} \rangle - \langle \alpha_{2-1}^{ex} \rangle\}$ contribution $[C(t)=0]$.

erage values of $R(\beta_A,t)$ are well described by Eq. (7.4) as can be seen in Fig. 17. This result is consistent with the near isotropic photoselection in a system where the ground and excited state degrees of alignment are close as indicated by the linear polarized excitation studies detailed above. At the bottom of the jet ϕ-dependent excitation measurements indicate the presence of some cylindrical asymmetry. In these circumstances there is the possibility of the creation of excited state $\langle \alpha_{2\pm1}^{ex} \rangle$ degrees of alignment from the presence of $\langle \alpha_{2\pm1}^{gs} \rangle$ and $\langle \alpha_{4\pm1}^{gs} \rangle$ moments of the ground state. $R(\beta_A,t)$ measurements following circularly polarized excitation at the bottom of the jet are shown in Fig. 18. The contrast between relaxation in cylindrically symmetric and asymmetric media is distinct, there is a marked time evolution in the individual $R(\beta_A,t)$ signals leading to a constant "relaxed" value after ≈ 6 ns for resorufin and 9 ns for rhodamine 6G. Circularly polarized excitation provides little displacement of the initial excited state distribution from that of the ground state and the evolution of the anisotropy in the conventional analyzer setting ($\beta_A = 0°$) which is only sensitive to $\langle \alpha_{20}^{ex} \rangle$ or $\langle \alpha_{2\pm2}^{ex} \rangle$ dynamics points to an inequality in the ground and excited state equilibrium degrees of alignment (linearly polarized excitation studies show no strong evidence for alignment cross
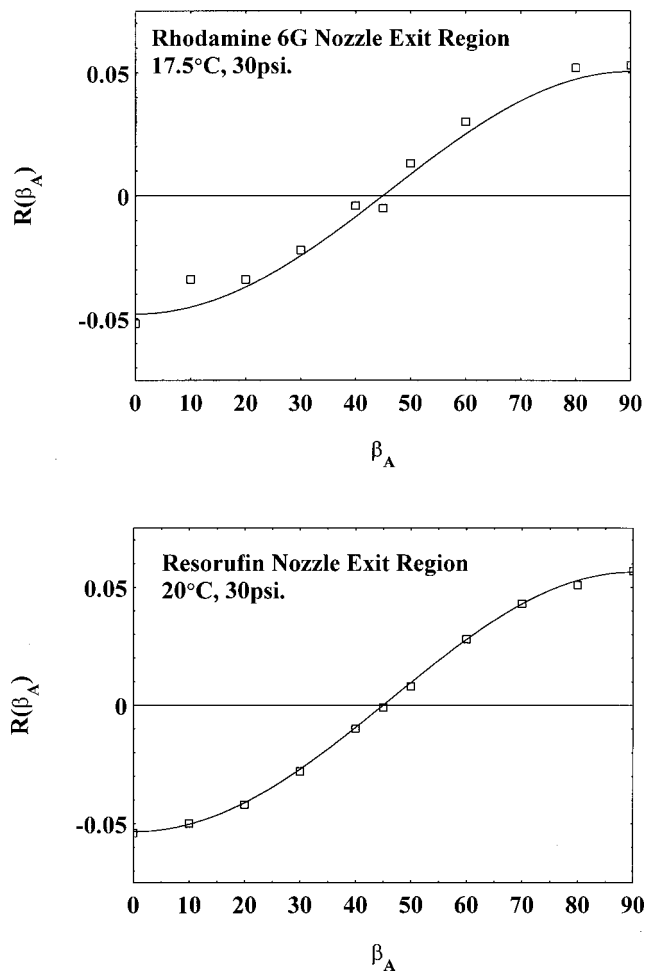
relaxation). Similar evolution in $R(\beta_A,t)$ is observed as β_A is increased to 90° it is clear that the initial and relaxed anisotropy data does not follow Eq. (7.4) and indicates the presence of $\langle \alpha_{2\pm1}^{ex} \rangle$ degrees of excited state alignment. Least-squares fits to the angular variation of the two anisotropies using Eq. (7.2) are shown in Fig. 19. For both molecules $C(t)$ shows substantial evolution with $C(ss)/C(0)$ in the region of 0.6. As the diagonal relaxation dynamics are dominated by the diffusion operator, the relationship between γ_{22} and γ_{21} is given by

$$\gamma_{22} = 2D_\perp + 4D_\parallel,$$

$$\gamma_{21} = 5D_\perp + D_\parallel. \tag{7.5}$$

The values of $D_\perp$ and $D_\parallel$ have already been determined from the linearly polarized experiments above and can be used to predict the γ_{21} decay rates which are displayed in Table IV. Given the small contribution of ϕ-diffusion to the $\langle \alpha_{2\pm1}^{ex} \rangle$ dynamics these values are close to those for γ_{20}. The evolution of $C(t)$ should therefore follow
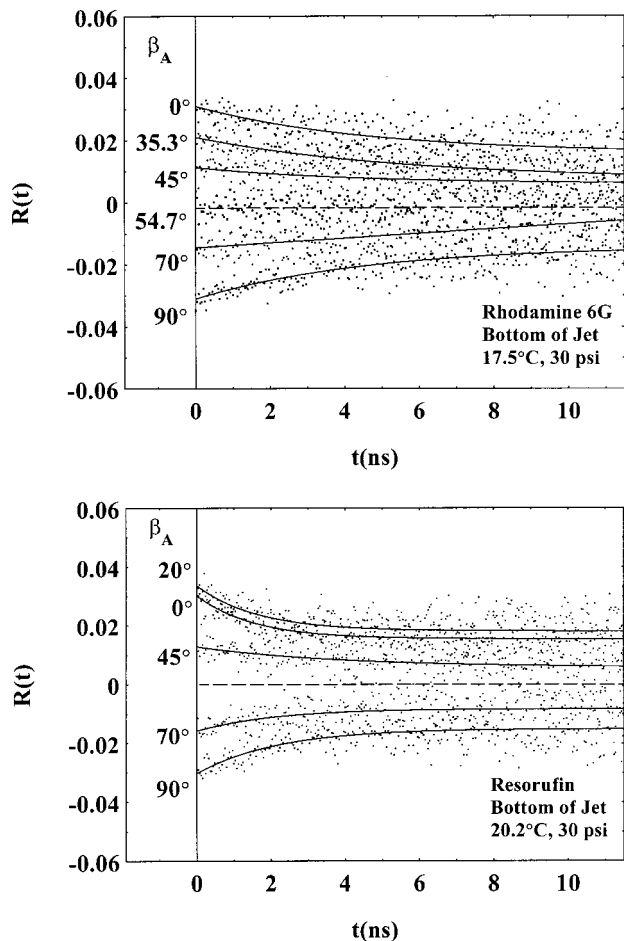
FIG. 18. Circularly polarized fluorescence anisotropy signals recorded at the bottom of the jet nozzle exit region for varying values of β_A. The behavior here is in contrast to that observed in the nozzle exit region in that there is a clear evolution of $R(t,\beta_A)$ to a steady state value. The solid line exponential fits to the data are intended as a guide to the eye and are not based on any model for the dynamics in this environment.

$$C(t) = \frac{2[\Lambda_{21}(0)\exp(-(5D_{\parallel}+D_{\perp})t)+\Lambda_{21}(ss)]}{\sqrt{30}+2[\Lambda_{22}(0)\exp(-(2D_{\parallel}+4D_{\perp})t)+\Lambda_{22}(ss)]},$$

where

$$\Lambda_{21}(0) = \{\{\langle\alpha_{21}^{ex}(0)\rangle - \langle\alpha_{2-1}^{ex}(0)\rangle\}$$
$$-\{\langle\alpha_{21}^{ex}(ss)\rangle - \langle\alpha_{2-1}^{ex}(ss)\rangle\}\},$$

$$\Lambda_{21}(ss) = \{\langle\alpha_{21}^{ex}(ss)\rangle - \langle\alpha_{2-1}^{ex}(ss)\rangle\},$$

$$\Lambda_{22}(0) = \{\{\langle\alpha_{22}^{ex}(0)\rangle - \langle\alpha_{2-2}^{ex}(0)\rangle\} \qquad (7.6)$$
$$-\{\langle\alpha_{22}^{ex}(ss)\rangle - \langle\alpha_{2-2}^{ex}(ss)\rangle\}\},$$

$$\Lambda_{22}(ss) = \{\langle\alpha_{22}^{ex}(ss)\rangle - \langle\alpha_{2-2}^{ex}(ss)\rangle\}.$$

Providing the $\{\langle\alpha_{22}^{ex}(t)\rangle + \langle\alpha_{2-2}^{ex}(t)\rangle\}$ dynamics are known [i.e., from $R(t,\beta)$ measurements] γ_{21} can be found. In principle the detailed form of $C(t)$ can be built up from a series of $R(\beta_A,t)$ curves; here, however, the noise levels that necessarily accompany a low fluorescence anisotropy preclude any detailed analysis. It is clear however that the initial value of the asymmetric alignment ratio is higher than the relaxed value for both dyes and that it is this additional parameter
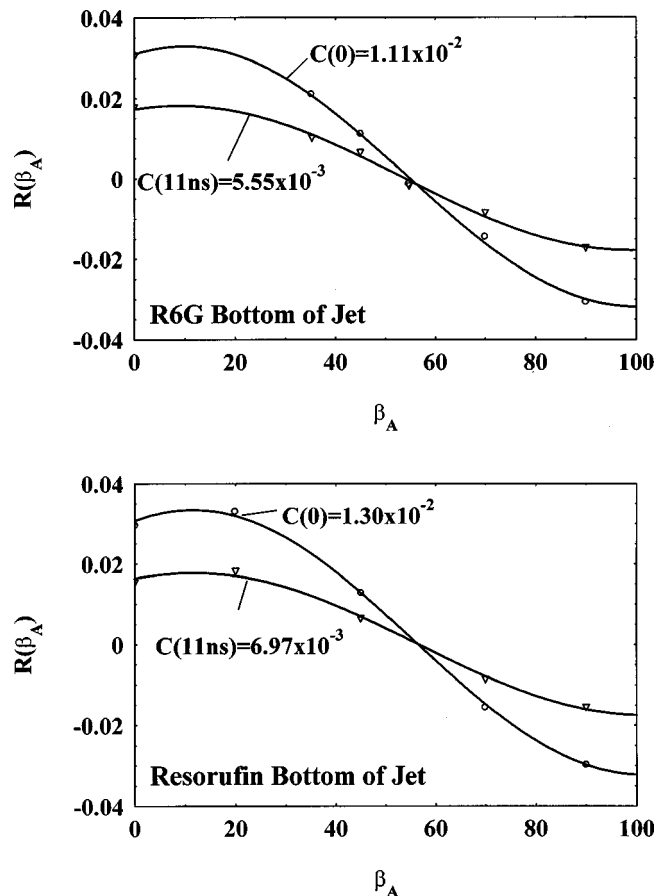

FIG. 19. Fits to the $R(t,\beta_A)$ data obtained in the positive alignment conditions found at the bottom of the jet. The initial and steady state values of the anisotropy [obtained by an average of the $R(t,\beta_A)$ signals about $t=11$ ns] indicates additional cylindrical asymmetry ($\{\langle\alpha_{2-1}^{ex}\rangle - \langle\alpha_{21}^{ex}\rangle\} \neq 0$) with an evolving ratio of the cylindrically asymmetric alignment.

that gives rise to the time dependence of $R(\beta_A,t)$ in the cylindrically asymmetric region of the jet. The use of circularly polarized excitation coupled with the measurement of the fluorescence anisotropy as a function of the analyzer axis nonetheless provides unequivocal evidence as to the degree of cylindrical symmetry of an aligned medium and the time evolution of $R(\beta_A,t)$ following circularly polarized excitation is seen to be an intrinsic property of a cylindrically asymmetric environment.

VIII. CONCLUSIONS

In this work we have shown how the use of (variable) linear and circular excitation polarizations in picosecond domain fluorescence anisotropy can be used to investigate both the order and full angular motion of a probe molecule in an anisotropic environment. The systems studied—jet aligned rhodamine 6G and resorufin—showed significant steady state alignment for the ground and excited states of both molecules to be present in the immediate transition from confined to free fluid flow. In this region the departure from isotropic relaxation dynamics is clearly visible, however, the $\langle\alpha_{20}^{ex}(t)\rangle$ and $\{\langle\alpha_{22}^{ex}(t)\rangle + \langle\alpha_{22}^{ex}(t)\rangle\}$ dynamics whilst unequal still remain linear as predicted by first order perturbation theory. From a consideration of the angular dependence of

the diffusion operator it was shown how the measurement γ_{20} and γ_{22} could be used to determine both the pure θ and ϕ diffusion rates. The results obtained point to an induced asymmetry in $D_\parallel$ and $D_\perp$ in the anisotropic regions of the jet which is attributed to flow induced changes in the solvent viscosity. At the nozzle exit with a negative steady state alignment ϕ-diffusion (motion in the alignment plane) is impeded with $D_\parallel \approx 0.8 D_\perp$; this relation is reversed with a change in steady state alignment at the bottom of the jet where $D_\parallel \approx 1.2 D_\perp$. In both instances motion in a perpendicular coordinate to that of the net alignment is favored. We have recently observed a similar although more pronounced diffusion anisotropy in the orientational dynamics of probe molecules doped into the nematic phase of a liquid crystal (5-cyano biphenyl) where with a net positive alignment of $\approx 20\%$ θ-diffusion ($D_\perp$) is significantly impeded ($A \cong 3.5$).[34,35]

The techniques developed in this work are applicable to the study of alignment dynamics in any anisotropic medium. To the best of our knowledge, this study represents the first direct determination of the full angular motion of fluorescent probes in an ordered environment.

ACKNOWLEDGMENTS

[1] A. J. Bain, P. Chandna, and G. Butcher-Taylor, postdeadline paper QPD-24 CLEO/QELS meeting, Baltimore, 1995.

[2] A. J. Bain, P. Chandna, and G Butcher, Chem. Phys. Lett. **260**, 441 (1996).

[3] J. C. Maxwell, Proc. R. Soc. London, Ser. A **22**, 46 (1873).

[4] M. Couette, Ann. Chim. Phys. **21**, 433 (1890).

[5] A. Peterlin and H. A. Stuart, Z. Phys. **112**, 1 (1939).

[6] H. G. Gerrard, Chem. Rev. **59**, 345 (1959).

[7] W. Heller, R. Tabiban, M. Nakagaki, and L. Papazian, J. Chem. Phys. **52**, 4294 (1970).

[8] J. Kerr, Philos. Mag. **50**, 337 (1875).

[9] G. Weber, J. Chem. Phys. **43**, 521 (1965).

[10] A. D. Buckingham, in *Molecular Electro-Optics*, edited by C. T. O'Konski (Marcel Dekker, New York, 1976), Part 1.

[11] I. Tinocho, Jr., J. Am. Chem. Soc. **77**, 4486 (1955).

[12] E. D. Cehelnik, R. B. Cundall, C. J. Timmons, and R. M. Bowley, Proc. R. Soc. London, Ser. A **335**, 387 (1973).

[13] D. A. Mc.Quarrie, *Statistical Mechanics* (Harper Collins, New York, 1976).

[14] A. J. Kenyon, A. J. McCaffery, C. M. Quintella, and J. F. Winkel, Mol. Phys. **72**, 965 (1991).

[15] A. J. Kenyon, A. J. McCaffery, C. M. Quintella, and J. F. Winkel, Mol. Phys. **74**, 871 (1991).

[16] T. Tao, Biopolymers **8**, 609 (1969).

[17] T. J. Chuang and K. B. Eisenthal, Chem. Phys. Lett. **11**, 368 (1971).

[18] J. C. Gumy and E. Vauthy, J. Phys. Chem. **100**, 8628 (1996).

[19] G. Butcher, Ph.D. thesis, University of Essex, 1995.

[20] K. G. Spears and K. M. Steinmetz, J. Phys. Chem. **89**, 3623 (1985).

[21] D. V. O'Connor and D. M. Phillips, *Time Correlated Single Photon Counting* (Academic, London, 1984).

[22] H-P. Harri, S. Leutwyler, and E. Schumacher, Rev. Sci. Instrum. **53**, 1855 (1982).

[23] P. Chandna, Ph.D. thesis, University of Essex, 1995.

[24] A. J. Bain and R. Dean (unpublished).

[25] J. N. Israelachvili, *Intermolecular and Surface Forces* (Academic, London, 1985).

[26] P. R. Hammond, J. Chem. Phys. **70**, 3884 (1979).

[27] R. J. D. Miller, M. Pierre, and M. D. Fayer, J. Chem. Phys. **78**, 5138 (1983).

[28] G. A. Kenny-Wallace, S. Payone, and C. Kalpouzos, Faraday Discuss. Chem. Soc. **85**, 185 (1988).

[29] D. S. Kliger, J. W. Lewis, and C. E. Randall, *Polarized Light in Optics and Spectroscopy* (Academic, San Diego, 1990).

[30] I. N. Dozov and I. I. Penchev, J. Lumin. **22**, 69 (1980).

[31] M. A. Taylor, D. N. Batchelder, and J. O'Dell, Polym. Compos. **29**, 253 (1988).

[32] I. Teraoka and R. Hayakawa, J. Chem. Phys. **91**, 7951 (1989).

[33] D. Baalas and S. Heft, Phys. Rev. Lett. **57**, 86 (1986).

[34] A. J. Bain, J. Bryant, and R. J. Dean, Proceedings of IQEC 1998, OSA Technical Digest Series, Vol. 7, 98 (1998) (unpublished).

[35] A. I. Bain and J. Bryant, Proceedings of QELS 1999, OSA Technical Digest Series, p. 185 (1999) (unpublished).